Review of Scientific Instruments

Analysis of the sharpening effect in gyromagnetic nonlinear transmission lines using the unidimensional form of the Landau–Lifshitz–Gilbert equation

Cite as: Rev. Sci. Instrum. **93**, 065101 (2022); https://doi.org/10.1063/5.0087452
Submitted: 05 February 2022 • Accepted: 16 May 2022 • Published Online: 02 June 2022

Ana F. G. Greco, José O. Rossi, Joaquim J. Barroso, et al.

Review of Scientific Instruments ARTICLE scitation.org/journal/rsi

Analysis of the sharpening effect in gyromagnetic nonlinear transmission lines using the unidimensional form of the Landau–Lifshitz–Gilbert equation

Cite as: Rev. Sci. Instrum. 93, 065101 (2022); doi: 10.1063/5.0087452
Submitted: 5 February 2022 • Accepted: 16 May 2022 •
Published Online: 2 June 2022

Ana F. G. Greco,[1] José O. Rossi,[1,a)] Joaquim J. Barroso,[1] Fernanda S. Yamasaki[1] André F. Teixeira,[1] Elizete G. L. Rangel[1] Lauro P. S. Neto,[2] and Edl Schamiloglu[3]

AFFILIATIONS

[1] National Institute for Space Research (INPE), São José dos Campos, SP 12227-010, Brazil
[2] Federal University of São Paulo (UNIFESP), São José dos Campos, SP 12247-014, Brazil
[3] University of New Mexico (UNM), Albuquerque, New Mexico 87131, USA

[a)] **Author to whom correspondence should be addressed:** jose.rossi@inpe.br

ABSTRACT

Continuous nonlinear transmission lines (NLTLs), also known as gyromagnetic lines, consist of ferrite-based magnetic cores biased by an external magnetic field. Over the past years, many analytical and experimental studies have predicted the rise time reduction of the input pulse to the range of a few nanoseconds or even hundreds of ps experimentally observed in such gyromagnetic lines. This effect, known as pulse sharpening, is investigated in this paper built on a model based on a periodic structure of inductive–capacitive cells in series with magnetization-driven voltage sources expressed by the one-dimensional form (1D) of the Landau–Lifshitz–Gilbert (LLG) gyromagnetic equation. We explore the model through parametric study under various input–pulse parameters to understand the physics behind the ferrimagnetic material responses. Moreover, the numerical results obtained from computational simulations using Mathematica (v. 12.1) show how the line parameters (input voltage, damping constant, saturation magnetization, and length) affect the sharpening effect, which is quantified by the switching time. Our results on ferrite-loaded coaxial lines have confirmed many results found in the literature. We validated with a good agreement the proposed model with the result obtained by Dolan in 1993 using the same 1D form of the LLG equation, thus showing that the model proposed here is suitable to quantify the sharpening effect produced by a gyromagnetic NLTL.

I. INTRODUCTION

Ferrite-loaded coaxial lines are a type of nonlinear transmission line (NLTL), being investigated since the 1960s motivated by the possibility of reducing the rise time of the input pulse to the range of some ns or even hundreds of ps. This effect is also known as pulse sharpening and occurs due to the dependence of magnetic permeability on the current amplitude and is used in several applications, such as laser-firing, ultra-wideband radar, and electronic beam control.[1–11]

In this work, we analyze the pulse sharpening effect by varying the characteristic values of several line parameters through a model based on the periodic structure of discrete inductive–capacitive cells in series with voltage sources, where the circuit equations are coupled with the one-dimensional (1D) form of the Landau–Lifshitz–Gilbert (LLG) equation. In this model, each section k of the discretized LTNL produces a coupled system of first order ordinary differential equations in the time domain, which relate the state variables: voltage V_k, current I_k, and magnetization M_k, all individually indexed. The proposed model is based on the work of Dolan,[12] who solved the coupled system of equations through the Transmission Line Modeling (TLM) method. However, in this work, the model is solved numerically through an iterative algorithm implemented in Mathematica (v. 12.1),[13] which has a set of specific

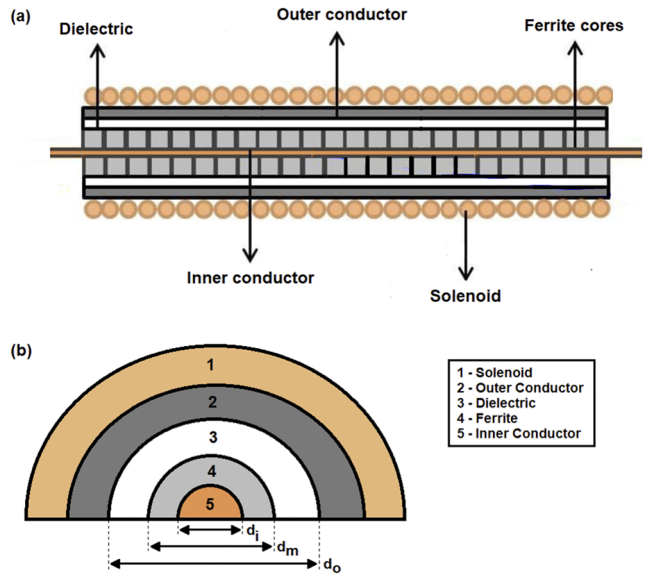

FIG. 1. (a) Schematic of a gyromagnetic NLTL. (b) Cross-sectional view of a gyromagnetic line, where d_i, d_m, and d_o represent the outer diameters of the inner conductor, ferrite ring, and dielectric layer, respectively.

tools for solving differential equations, such as the NDSolve function used to solve the system of equations.

This paper is organized as follows: in Sec. II, some concepts related to gyromagnetic NLTLs are presented, followed in Sec. III with the proposed formulation, and discussed and validated in Secs. IV and V through simulation results. Finally, in Sec. VI, the final considerations are made.

II. BASIC CONCEPTS OF GYROMAGNETIC NLTLS

A. General structure

A gyromagnetic line is a coaxial structure consisting of ferrite rings inserted into the inner conductor, a dielectric to insulate the ferrite from the outer conductor, and a solenoid that produces a magnetic field to bias the line. Figures 1(a) and 1(b) show the line schematic and cross-sectional view, respectively.[14]

B. Principle of operation

The principle of operation of the gyromagnetic line is based on the nonlinear behavior of the magnetic material that fills the line along its length. As the injected input pulse travels along the line, the magnetic permeability of ferrite decays rapidly with the amplitude of the current, thus increasing the propagation velocity. The inverse relationship between the propagation velocity and magnetic permeability allows the top of the pulse to travel faster than its base, reducing the pulse rise-time. This effect is known as rise-time reduction or pulse sharpening,[15] as pictured in Fig. 2.

An analysis of the development and propagation of the electromagnetic shock formed in an NLTL was given by Katayev,[2] where it is shown that the rise time for the shock front (10%–90%) is equivalent to the ferrite switching time and can be estimated by[2,16]

$$\tau_{sh} = \frac{6.7 \cdot (1+\alpha^2)}{\alpha \cdot \gamma . \mu_0 . H_{sh}}, \tag{1}$$

where the damping parameter α is a dimensionless number, γ is the gyromagnetic ratio of the electron (1.76×10^{11} rad/s/T), μ_0 is the permeability of the vacuum ($4\pi \times 10^{-7}$ H/m), and H_{sh} is the peak magnetic field amplitude defined in terms of the effective diameter d_{ef} of the ferrite ring and the peak current amplitude I_{sh},

$$H_{sh} = \frac{1}{r_m - r_i}\int_{r_i}^{r_m} \frac{I_{sh}}{2\pi r} dr = \frac{I_{sh}}{\pi d_{ef}}, \tag{2}$$

where $d_{ef} = (d_m - d_i)/\ln(d_m/d_i)$ and the peak current amplitude I_{sh} can be obtained from the peak voltage on the load or by directly measuring the current in the line inductive–capacitive (LC) sections in the simulation.

III. MODELING OF GYROMAGNETIC NLTL

A. General model of a transmission line

The vast majority of approaches to modeling the continuous gyromagnetic line use as a reference a lumped-parameter network proposed by Dolan.[12,14] The sections of such a discrete ladder network consist of a shunt capacitance and a series inductance connected to a magnetization-driven source voltage determined by the time rate of change of the magnetic flux through the ferrite rings (Fig. 3).

For the case of wave propagation with electric and magnetic fields without longitudinal components, called the transverse electromagnetic mode (TEM), Faraday's and Ampere's laws give the spatiotemporal variations of the line voltage and current as[14]

$$\frac{dI}{dz} = C_0 \frac{dV}{dt}, \tag{3}$$

$$\frac{dV}{dz} = L_0 \frac{dI}{dt} + \frac{d\phi_m}{dt}, \tag{4}$$

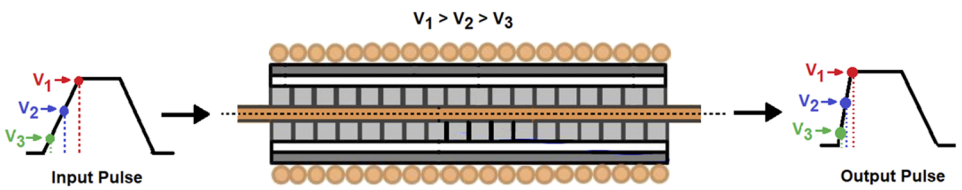

FIG. 2. Sharpening effect produced in a gyromagnetic NLTL.

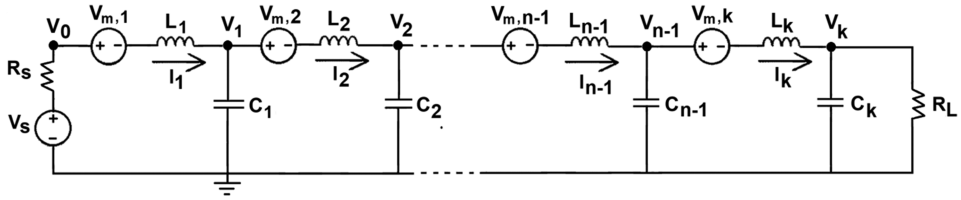

FIG. 3. The circuit model representing a gyromagnetic NLTL, where the state variables considered are the current I_k in the inductor of section k, the voltage V_k in the capacitor of section k, and the source voltage $V_{m,k}$ due to the magnetization M_k in section k. Although lumped in the upper conductor, L_k and V_k actually encompass the net effect of both conductors in each line section.

where I represents the current, V is the voltage, and C_0 and L_0 are the linear capacitance and inductance per unit of length, expressed, respectively, by[17]

$$C_0 = \frac{2\pi\varepsilon_0}{\frac{1}{\varepsilon_d}\ln\left(\frac{d_0}{d_m}\right) + \frac{1}{\varepsilon_f}\ln\left(\frac{d_m}{d_i}\right)}, \tag{5a}$$

$$L_0 = \frac{\mu_0}{2\pi}\left[\mu_d \ln\left(\frac{d_0}{d_m}\right) + \mu_{fs}\ln\left(\frac{d_m}{d_i}\right)\right], \tag{5b}$$

where ε_0, ε_d, and ε_f represent, respectively, the permittivities of the vacuum, dielectric, and ferrite and μ_d and μ_{fs} are the permeability of the dielectric and ferrite in saturation, respectively. In addition to the linear magnetic flux $L_0 I$ in Eq. (4), the magnetization component per unit length of the total flux linkage coupling the inner and outer coaxial conductors is[14]

$$\phi_m = \int_{d_i/2}^{d_m/2} \mu_0 M_\theta(r)dr = \mu_0\left(\frac{d_m - d_i}{2}\right)M_\theta, \tag{6}$$

where M_θ represents the circumferential component of the magnetization assumed to be constant in the radial direction.[12,14]

Hence, the rate of change of the magnetic flux in (4) is rewritten as[14]

$$\frac{dV}{dz} = L_0\frac{dI}{dt} + \mu_0\left(\frac{d_m - d_i}{2}\right)\frac{dM_\theta}{dt}, \tag{7}$$

where $\frac{dM_\theta}{dt}$ is the rate of change of magnetization in the circumferential direction, obtained directly from the 1D form of the LLG equation,[12,18]

$$\frac{dM_\theta}{dt} = \alpha\frac{\gamma}{1+\alpha^2}\mu_0 M_s H_\theta\left(1 - \frac{M_\theta^2}{M_s^2}\right), \tag{8}$$

where M_s represents the saturation magnetization and H_θ is the circumferential magnetic field averaged over the radial thickness of the ferrite bead. We see that the magnetic field term H_θ in the LLG Eq. (8) embodies the effect of the line current on the ferrite magnetization, whereas dM_θ/dt determines the voltage V_k in the transmission line network (Fig. 3).

We remark that although the magnetization varies in three dimensions, the proposed model uses the 1D form of the LLG equation, in which only the circumferential magnetization component contributes to the flux variation in the TEM mode since the radial and axial components are compensated by demagnetizing fields.[14]

B. Description of the proposed 1D model

The developed model is based on the work proposed by Dolan,[12] where the effects of the magnetization of ferrite, represented by the voltage sources as nonlinear elements, are expressed using the 1D form of the LLG equation. Figure 3 shows a schematic for the proposed model.

Of importance from a numerical point of view, the variables described in the circuit are such that the differential equations are all first-order. Therefore, considering each of the NLTL sections, we arrive at a system of ordinary differential equations with three variables, separated into initial, intermediate, and final sections, coupling the two basic equations of a transmission line for voltage and current with the 1D form of the LLG equation.

Initial section:

$$\begin{cases} \dfrac{dV_k}{dt} = \dfrac{I_k}{C_k} - \dfrac{I_{k+1}}{C_k}, \\ \dfrac{dI_k}{dt} = \dfrac{V_s}{L_k} - \dfrac{V_k}{L_k} - R_s\cdot\dfrac{I_k}{L_k} - \dfrac{1}{L_0}.\dfrac{\mu_0}{2}\cdot(d_m - d_i).\dfrac{dM_k}{dt}, \\ \dfrac{dM_k}{dt} = \alpha.\dfrac{\gamma}{1+\alpha^2}.\mu_0.M_s.\dfrac{I_k}{\pi.d_{ef}}.\left(1 - \dfrac{M_k^2}{M_s^2}\right), \\ k = 1, \end{cases} \tag{9}$$

where M_k represents the magnetization of the kth element and C_k and L_k are the capacitance and inductance per section, expressed, respectively, by

$$C_k = \frac{C_0.l}{n}, \tag{10a}$$

$$L_k = \frac{L_0.l}{n}, \tag{10b}$$

where l represents the line length and n is the total number of sections.

Intermediate sections:

$$\begin{cases} \dfrac{dV_k}{dt} = \dfrac{I_k}{C_k} - \dfrac{I_{k+1}}{C_k}, \\ \dfrac{dI_k}{dt} = \dfrac{V_{k-1}}{L_k} - \dfrac{V_k}{L_k} - \dfrac{1}{L_0}.\dfrac{\mu_0}{2}\cdot(d_m - d_i).\dfrac{dM_k}{dt}, \\ \dfrac{dM_k}{dt} = \alpha.\dfrac{\gamma}{1+\alpha^2}.\mu_0.M_s\cdot\dfrac{I_k}{\pi.d_{ef}}.\left(1 - \dfrac{M_k^2}{M_s^2}\right), \\ k = 2, 3, \ldots, n-1. \end{cases} \tag{11}$$

Final section:

$$\begin{cases} \dfrac{dV_k}{dt} = \dfrac{I_k}{C_k}, \\ \dfrac{dI_k}{dt} = \dfrac{V_{k-1}}{L_k} - \dfrac{V_k}{L_k} - R_L \cdot \dfrac{I_k}{L_k} - \dfrac{1}{L_0}.\dfrac{\mu_0}{2} \cdot (d_m - d_i).\dfrac{dM_k}{dt}, \\ \dfrac{dM_k}{dt} = \alpha . \dfrac{\gamma}{1+\alpha^2} . \mu_0 . M_s . \dfrac{I_k}{\pi . d_{ef}} . \left(1 - \dfrac{{M_k}^2}{{M_s}^2}\right), \\ k = n. \end{cases} \tag{12}$$

C. Numerical solution from the proposed model

The literature gives different methods for the numerical solution of the set of Eqs. (9)–(12). For example, Dolan[12,14] solved this coupled set of equations using the Transmission Line Matrix (TLM) method with each LC section, represented in Fig. 3, replaced by an equivalent transmission line section with its characteristic impedance $Z_0 = \sqrt{L_0/C_0}$ and transit time $\tau = \Delta z\sqrt{L_0 C_0}$. This method adopted by Dolan has similarities with a method in Ref. 19, the Finite Difference Time Domain (FDTD) method. However, the main difference is that the TLM is a physical model based on electrical circuits, while the FDTD is a mathematical model based on Maxwell's equations.

As a paper's contribution, the system of coupled Eqs. (9)–(12) is solved numerically in the Mathematica software (v. 12.1),[13] through the NDSolve built-in command subject to given initial conditions. Figure 4 shows a flow chart for the algorithm implemented in Mathematica. A program script detailing the NDSolve command and the discretization model is available as the supplementary material.

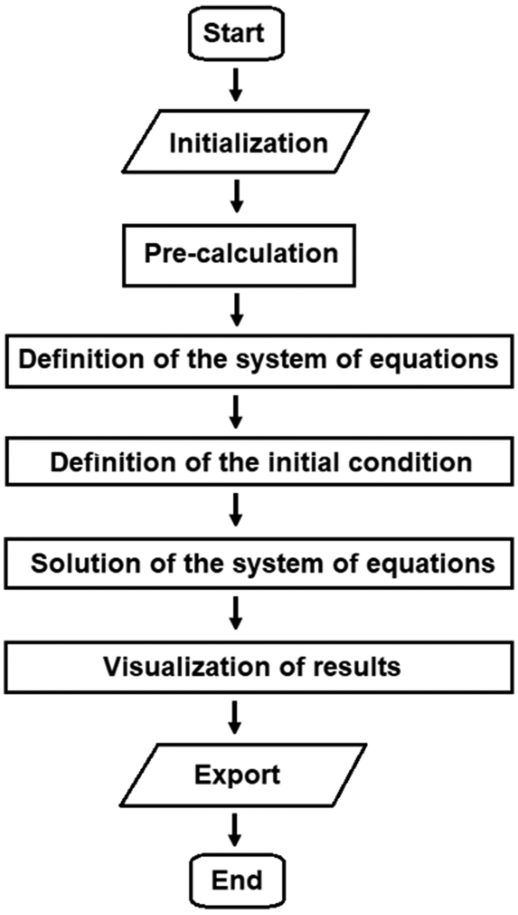

FIG. 4. Flowchart of the algorithm implemented in Mathematica.

IV. ANALYSIS OF THE SHARPENING EFFECT

A. Definition of simulation parameters

For the pulse sharpening analysis, we modeled a lossless nickel–zinc (NiZn) gyromagnetic NLTL fed by a Gaussian-shaped pulse of a 15 kV amplitude with a 25 ns duration. The circuit model also has a generator resistance and load, both of 60 **Ω**, matched to the line characteristic impedance. Table I gives the main simulation parameters.

The permeability and permittivity of ferrite and dielectric, as well as the outer diameters of the inner conductor, ferrite, and dielectric, are physical parameters of the line and were used to calculate the capacitance and inductance per unit of length and per section, defined by Eqs. (5a) and (5b) and (10a) and (10b), respectively. The number n of sections represents an important numerical parameter used to discretize the continuous gyromagnetic line. Thus, n should be of a sufficiently high value to avoid unwanted oscillations caused by the dispersive characteristics of the discretized line in the model. If n is too low, artifact oscillations can appear on the simulated wavefront, making the pulse highly oscillatory.[14,19]

In this way, to ensure simulation convergence and from the fact that the line behaves as a low-pass filter, the inverse of the Bragg frequency (f_{Bragg}) should be less than 10% of the estimated shock front rise time (t_{rf}), namely,[19]

$$\frac{1}{f_{Bragg}} < 0.1 t_{rf}, \tag{13}$$

where the Bragg frequency is expressed by $f_{Bragg} = 1/\pi\sqrt{L_k C_k}$.

TABLE I. Parameters used in the numerical simulations.

Parameter	Symbol	Value
Relative saturated permeability	μ_{fs}	5.0
Ferrite relative permittivity	ε_f	16.0
Relative permeability of the dielectric	μ_d	2.1
Relative permittivity of the dielectric	ε_d	1.0
Diameter of the inner conductor	d_i	0.8 mm
Ferrite outer diameter	d_m	1.4 mm
Outer diameter of the dielectric	d_o	2.5 mm
Effective diameter	d_{ef}	1.1 mm
Number of sections	n	138

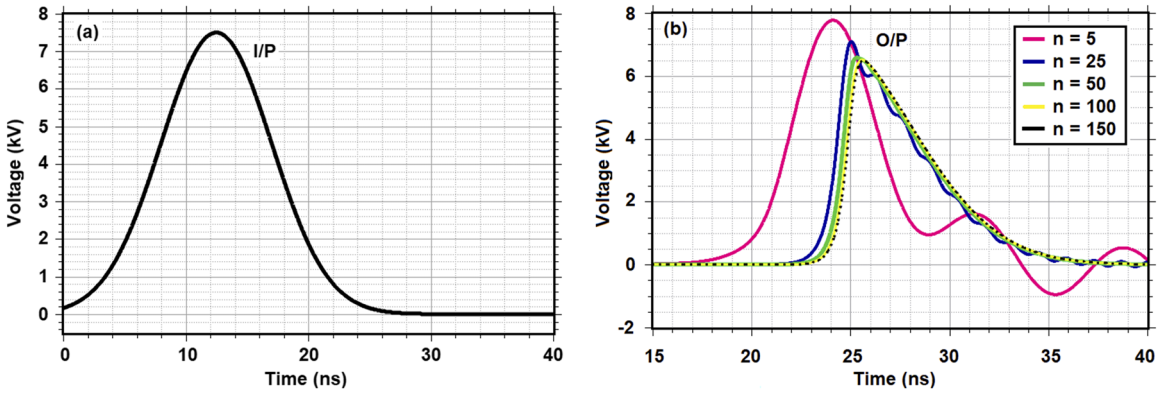

FIG. 5. (a) Gaussian input pulse and (b) output pulse for a varying number of sections.

Finally, based on the above expressions and using Eqs. (10a) and (10b), the number of sections n should satisfy

$$n > \frac{l\pi\sqrt{L_0 C_0}}{0.1 t_{rf}}. \tag{14}$$

Thus, considering l = 1 m, L_0 = 675.24 nH/m, C_0 = 0.18 nF/m, and t_{rf} ~ 2.5 ns, Eq. (14) gives about 138 sections for the required discretization. As shown in Fig. 5(b), for coarse discretization (n = 5), the output pulse shape is highly oscillatory. As the discretization is finer (n > 100), the simulations converge, demonstrating that the output response is due to actual magnetic resonance effects instead of the numerical artifacts.

In addition, Table II shows how simulation running time increases with the number of sections.

TABLE II. Dependence of simulation running time on the number of sections.

n	Time
5	00:02,34
25	00:07,24
50	00:27,76
100	01:31,16
150	02:52,08

B. Influence of input voltage (Vp) on the sharpening effect

The first parameter investigated was the input voltage whose simulation values ranged from 5 to 11 kV. Figure 6(a) shows the output temporal waveforms for increasing values of the input voltage, and Fig. 6(b) displays the variation of the output rise time with Vp.

From Fig. 6, we observe that increasing input voltage reduces both the delay and the rise time of the output pulse, making the pulse rising edge sharper. By noting that the input pulse has a rise time of ~12.50 ns, for the 5 kV pulse, for example, the rise time drops to ~4.87 ns, and for the 10 kV pulse, the time drops to ~2.11 ns, that is, a reduction of ~83% to the input pulse.

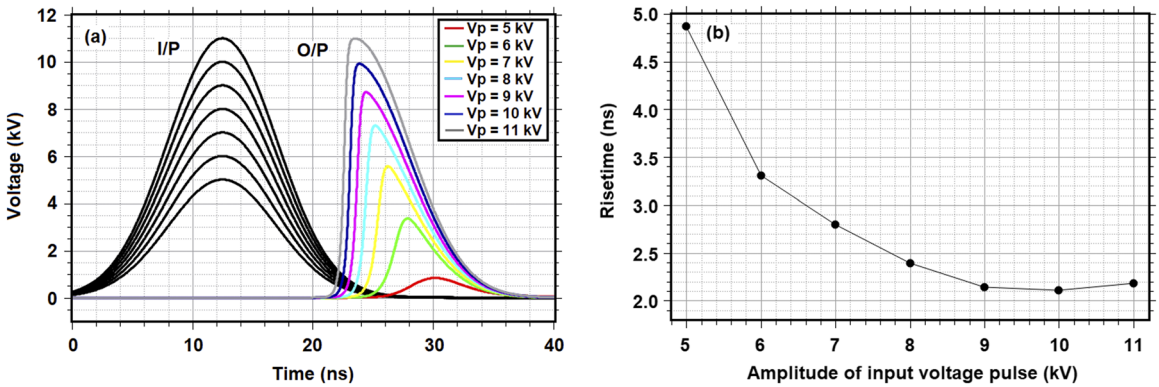

FIG. 6. (a) Comparison between the input and output pulses for different input voltage amplitudes as a function of time for a 1 m long gyromagnetic line. (b) Output rise time variation with input voltage. Remaining numerical simulation parameters are $\mu_0 M_s$ = 0.35 T, α = 0.5, and with the following initial conditions: I_k (t = 0) = V_k (t = 0) = M_k (t = 0) = 0.

TABLE III. Switching and rise times varying with the input voltage.

Input Voltage (kV)	Switching Time (ns)	Rise time (ns)
5	5.94	4.87
6	3.81	3.31
7	2.90	2.85
8	2.41	2.39
9	2.06	2.14
10	1.82	2.11
11	1.65	2.12

TABLE IV. Relationship between the current, magnetic field, and switching time for the input voltage.

Input voltage (kV)	Current (A/m)	Magnetic field (kA/m)	Switching time (ns)
5	43.0	12.77	5.94
6	67.0	19.89	3.81
7	88.0	26.13	2.90
8	106.0	31.47	2.41
9	124.0	36.81	2.06
10	140.0	41.56	1.82
11	155.0	46.02	1.65

Several authors have also observed that an increase in input voltage reduces the rise time. Weiner[20] and Furuya,[21] for example, simulated this effect using the 1D form of the LLG equation, Dolan[14] used the 3D form of the LLG equation[22], and recently Weihao[15] reported a simulation based on a line modeled by nonlinear inductors.

To verify the relationship between the simulated sharpening effect and the analytical switching time, τ_{sh}, we use Eqs. (1) and (2) to calculate τ_{sh} and compare it with the rise time measured from simulation, taking I_{sh} as the average of the currents calculated in five different sections. Table III gives this comparison.

Table III shows that the switching time and rise time are in good agreement for the 6–9 kV range, indicating the optimal rise time at 8 kV. In addition, observe that, although the input voltage does not appear explicitly in Eq. (1), this parameter has a strong influence on the switching time since the current that generates the magnetic field, in Eq. (1), is directly related with the voltage through the system of coupled equations [Eqs. (9)–(12)]. As a result of this interdependence, when the voltage increases, the current and the magnetic field also increase, thus decreasing the switching time, as given in Table IV.

C. Influence of the damping parameter (α) on the sharpening effect

The second parameter investigated was the dimensionless damping parameter, whose values for this simulation ranged between 0.001 and 1.0. Figure 7(a) shows the output temporal waveforms for increasing values of the damping parameter, and Fig. 7(b) displays the variation of the output rise time with α.

From Fig. 7, we observe that increasing alpha causes a continuous reduction in the rise time of the output pulse. In addition, we see in Fig. 7(a) that, for $\alpha > 0.5$, the output waveform barely changes, and the corresponding rise times remain nearly constant.

Dolan and Bolton[23] and recently Cui[24] did a similar analysis using the 3D form of the LLG equation where the line was polarized by an external magnetic field in an operating regime for high-power microwave generation. However, comparing those results with the ones obtained here is not convenient, as this article focuses only on the sharpening effect through the 1D form of the LLG equation, where there is no external axial polarization field.

Table V presents the comparison between the switching time calculated by Eqs. (1) and (2) and the rise time obtained through the simulations.

Table V shows that the switching time and rise time agree reasonably well for values between 0.25 and 1.0, yet for values between 0.001 and 0.1, the switching time becomes much longer than the rise

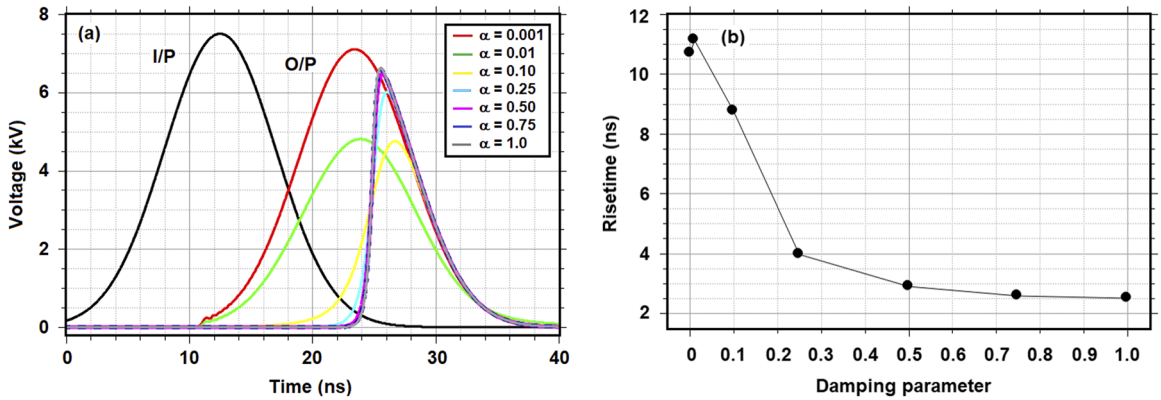

FIG. 7. (a) Comparison between the input and output pulses as a function of time for different alphas for a 1 m long gyromagnetic line. (b) Output rise time variation with the damping parameter. Remaining numerical simulation parameters are amplitude of the input pulse Vp = 7.5 kV, $\mu_0 M_s$ = 0.35 T, and with the following initial conditions: I_k $(t = 0) = V_k$ $(t = 0) = M_k$ $(t = 0) = 0$.

TABLE V. Switching and rise times varying with the damping parameter.

Damping parameter	Switching time (ns)	Rise time (ns)
0.001	865.17	10.70
0.01	120.12	11.14
0.10	12.73	8.75
0.25	4.47	3.97
0.50	2.61	2.90
0.75	2.17	2.58
1.00	2.08	2.39

TABLE VI. Variation of the proportionality factor and switching time with the damping parameter.

Damping parameter	Factor $\frac{(1+\alpha^2)}{\alpha}$	Switching time (ns)
0.001	1002.0	865.17
0.01	102.01	120.12
0.1	12.10	12.73
0.25	6.25	4.47
0.50	4.50	2.61
0.75	4.08	2.17
1.00	4.00	2.08

time obtained from the simulation. The justification is simple since analyzing the proportionality factor $\frac{(1+\alpha^2)}{\alpha}$ in Eq. (1), we note that the smaller the alpha value, the longer the switching time as this factor is too big. However, for $0.5 \leq \alpha \leq 1.0$, as given in Table VI, the damping parameter tends to stabilize around 0.5 and no longer significantly reduces the switching time.

TABLE VII. Switching and rise times varying with the saturation flux density.

Saturation flux density (T)	Switching time (ns)	Rise time (ns)
0.10	2.18	5.66
0.15	2.25	4.16
0.20	2.31	3.27
0.25	2.39	2.96
0.30	2.48	2.64
0.35	2.61	2.78
0.40	2.80	3.22

D. Influence of the saturation magnetization (M_s) on the sharpening effect

The third parameter investigated was the saturation magnetization M_s that relates to the saturation flux density by $B_s = \mu_0 M_s$ with values varying between 0.10 and 0.40 T in this simulation. Figure 8(a) shows the output temporal waveforms for increasing values of the saturation magnetization, and Fig. 8(b) displays the variation of the output rise time with the saturation flux density.

From Fig. 8, we observe that as the saturation magnetization increases, the pulse delay also increases. A similar analysis using the 3D form of the LLG equation was done by Dolan and Bolton[23] and recently by Cui,[24] and their results also indicate this trend. In addition, we note a continuous reduction in the output pulse amplitude with increasing M_s and a minimum rise time at $B_s = 0.30$ T. Table VII gives the comparison of the calculated switching time by Eq. (1) and the rise time obtained for this case.

Table VII shows that the switching time and rise time are in good agreement for the range of 0.25–0.35 T, indicating the optimal rise time of 2.64 ns at the saturation flux density $\mu_0 M_s = 0.30$ T. In addition, note that, although the saturation magnetization does not appear explicitly in Eq. (1), this parameter has some influence on the switching time, since the current that generates the magnetic field, in Eq. (1), is directly related to the saturation magnetization through the coupling of the LLG and circuit equations [Eqs. (9)–(12)]. As a

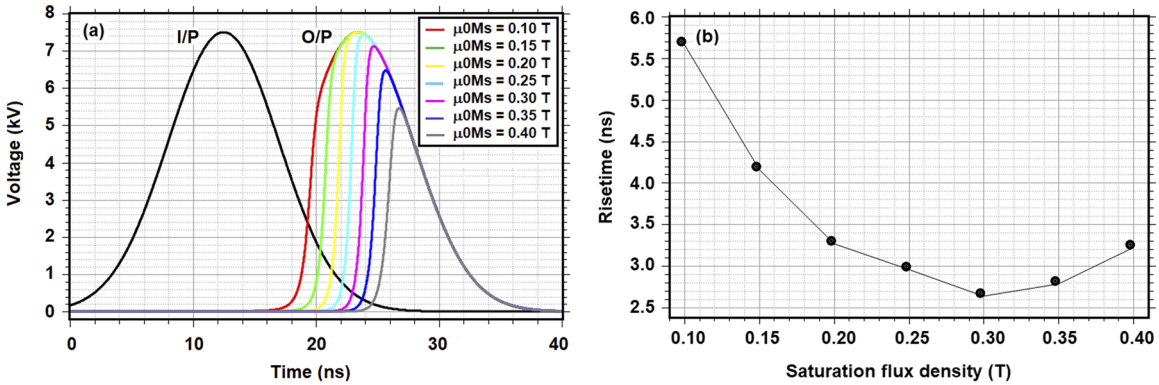

FIG. 8. (a) Comparison between the input and output pulses for different magnetizations as a function of time for a 1 m long gyromagnetic line. (b) Output rise time variation with saturation magnetization. Remaining numerical simulation parameters are the amplitude of the input pulse Vp = 7.5 kV, $\alpha = 0.5$, and with the following initial conditions: $I_k\,(t = 0) = V_k\,(t = 0) = M_k\,(t = 0) = 0$.

TABLE VIII. Variation of the current, magnetic field, and switching time with the saturation flux density.

Saturation flux density (T)	Current (A/m)	Magnetic field (kA/m)	Switching time (ns)
0.10	116.6	34.70	2.18
0.15	113.0	33.63	2.25
0.20	110.4	32.85	2.31
0.25	106.4	31.66	2.39
0.30	102.6	30.51	2.48
0.35	97.6	29.05	2.61
0.40	91.0	27.01	2.80

result of this interdependence, with increasing M_s, the current and magnetic field both decrease, thus increasing the switching time, as given in Table VIII.

E. Influence of the line length (*l*) on the sharpening effect

The fourth and last parameter investigated was the line length, whose values for this simulation vary between 0.20 and 1.20 m. Figure 9(a) shows the output temporal waveforms for increasing values of the line length, and Fig. 9(b) displays the variation of the output rise time with *l*.

From Fig. 9, we see that as the line length increases, the pulse delay also increases and the output pulse amplitude remains nearly constant up to 0.60 m and then tends to decrease. This effect was also observed by Dolan[14] and indicates that the length of the line should be increased with the amplitude of the input pulse to prevent the output pulse amplitude from decreasing. In practice, this means that longer lines require higher voltages.

In addition, the pulse rise time gradually decreases and then slightly increases after reaching a minimum rise time at the line length of 0.80 m. Many works[14,20,21] demonstrate this effect, for which there is an optimal length and that if the line length exceeds this value, the rise time will remain roughly unchanged or, perhaps, slightly increased due to line dispersion effects.

TABLE IX. Switching and rise times varying with the line length.

Length (m)	Switching Time (ns)	Rise time (ns)
0.20	2.06	7.18
0.40	2.30	4.66
0.60	2.40	3.28
0.80	2.53	2.76
1.00	2.60	2.86
1.20	2.79	3.08

TABLE X. Variation of the current, magnetic field, and switching time with the line length.

Length (m)	Current (A/m)	Magnetic field (kA/m)	Switching time (ns)
0.20	124.0	36.81	2.06
0.40	111.0	32.95	2.30
0.60	107.0	31.77	2.40
0.80	100.8	29.93	2.53
1.00	98.0	29.09	2.60
1.20	91.4	27.14	2.79

Note that, for a short line of 0.20 m, for example, only around 10 ns, the initial rising edge of the pulse is sharpened. Table IX gives the comparison of the calculated switching time given by Eq. (1) and the rise time obtained from the simulation.

Table IX indicates that as the line increases, the optimal length is reached at 0.80 m, which corresponds to the minimum rise time of 2.76 ns in the input voltage amplitude of 7.5 kV considered in this case. Furthermore, the calculation for the switching time agrees well with the measured rise time only if the line length is equal to or greater than the optimal line length.

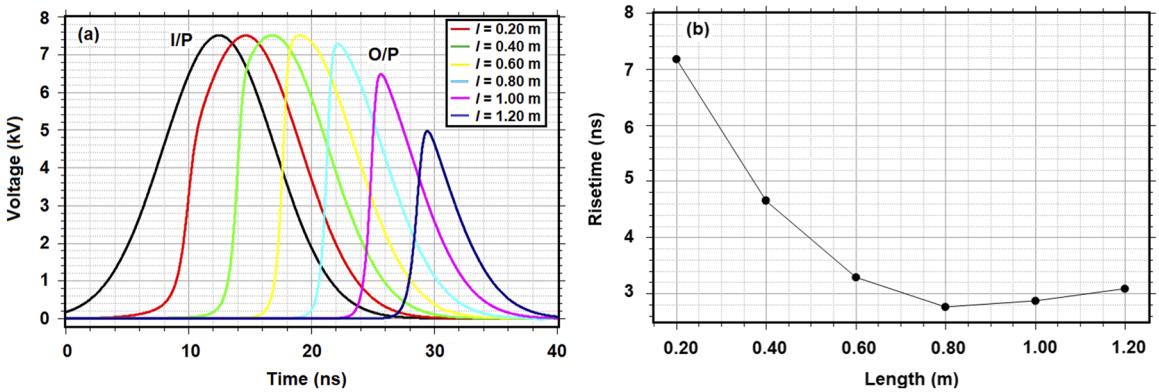

FIG. 9. (a) Comparison between the input and output pulses for different lengths as a function of time for a gyromagnetic line. (b) Output rise time variation with length. Remaining numerical simulation parameters are amplitude of the input pulse Vp = 7.5 kV, $\mu_0 M_s$ = 0.35 T, α = 0.5, and with the following initial conditions: I_k (t = 0) = V_k (t = 0) = M_k (t = 0) = 0.

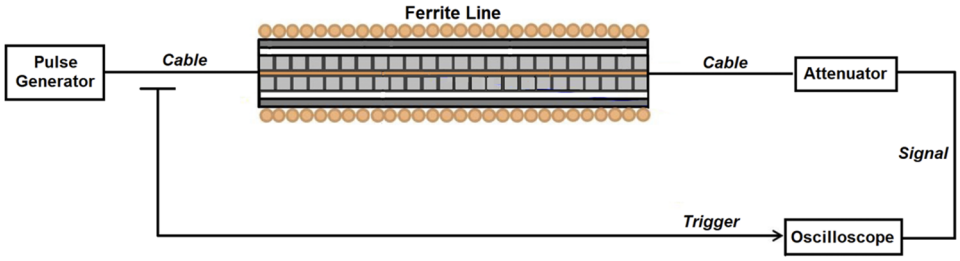

FIG. 10. Schematic arrangement of a ferrite-filled line.

Although the line length does not appear explicitly in Eq. (1), this parameter has some influence on the magnetization dynamics, since the lumped capacitive and inductive elements C_k and L_k, which are embodied in the system of coupled Eqs. (9)–(12), are directly related with the line length through Eq. (10). As a result of this interdependence, as the length increases, the current and magnetic field both decrease, thereby increasing the switching time, as given in Table X.

V. VALIDATION

To validate the predictions of the proposed model, we performed a numerical simulation based on the work by Dolan,[12] using the 1D form of the LLG equation and made a comparison with experimental data. In this work,[12] the experimental line consisted of manganese–zinc (MgZn) ferrite beads, with inner conductor outer diameter d_i = 1.2 mm, ferrite outer diameter d_m = 3.5 mm, with a total length of 11.0 cm and saturation flux density $\mu_0 M_s$ = 0.38 T, and surrounded by a dielectric conductor with 4.5 mm in diameter, thus forming an insulating layer. This line was connected at the input to a pulse generator with a negative voltage amplitude of 9.2 kV via a 50 Ω coaxial cable and at the output by 20 GHz coaxial attenuators, allowing measurements through a digital oscilloscope. A schematic of the implemented line is shown in Fig. 10.

TABLE XI. Parameters used for validation.

Parameters	Symbol	Value
Relative permeability of the saturated ferrite	μ_{fs}	2.0
Ferrite relative permittivity	ε_f	16.0
Relative permeability of the dielectric	μ_d	2.1
Relative permittivity of the dielectric	ε_d	2.0
Damping parameter	α	0.5
Number of sections	n	92

Therefore, taking the information described above as a reference, the model was evaluated considering the parameters in Table XI from Dolan's work.[12]

Figure 11(a) shows the comparison between the simulated and experimental results presented by Dolan,[12] and Fig. 11(b) displays the numerical result reproduced in this work.

We see in Fig. 11(a) that the simulated and the experimental results presented by Dolan have a good fitting between them. In addition, we verify from Figs. 11(a) and 11(b) that the delay and amplitude for the output pulses of our simulation model agree reasonably well, with the leading edge of the original pulse decaying slightly faster than that of the reproduced pulse. In Ref. 12, the reduction in the rise time for the output pulse was ~2 ns, whereas, for the reproduced pulse, the rise-time reduction was ~3 ns. As the rise time indirectly depends on the input pulse amplitude, perhaps this difference in rise-time (original and reproduced) can be

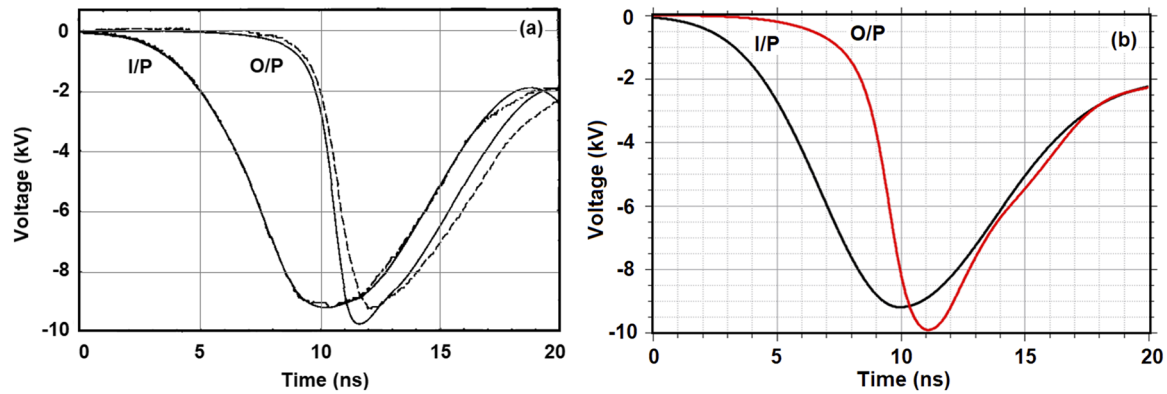

FIG. 11. Comparison between I/P input and O/P output pulses. (a) Original, where the dashed line is the experimental measurement and the solid line is the simulated result. Reproduced with permission from Electronic Letters 29, 9 (1993). Copyright 1993, IET. (b) Reproduction of the original simulated waveform using our code with the initial conditions: $I_k\ (t = 0) = V_k\ (t = 0) = M_k\ (t = 0) = 0$.

justified by the type of pulse waveform at the input on the line. Dolan's work gives no mention of the input pulse shape used. However, we assumed it was represented by a polynomial function of the third degree since he used the cubic interpolation method. On the other hand, our work models the input pulse using a Gaussian function that fits the simulation well. In addition, Dolan did not provide any information in his work about some parameters of the line, defined in Table XI. Thus, we cannot fully reproduce the original result with accuracy. However, our results show that the model used in this work can generate the sharpening effect in a gyromagnetic NLTL.

VI. CONCLUSION

Since the 1960s, the sharpening effect produced in gyromagnetic NLTLs through practical experiments and numerical simulations has been studied in several works. In this paper, we have also investigated this effect based on a numerical discretization modeling of a ferrite-loaded coaxial structure using a ladder network with circuit equations for current and voltage coupled to the 1D form of the LLG equation. A total of four design parameters of the ferrite line varied in the simulation showed that the obtained results indicate a strong influence on the sharpening effect. Furthermore, the results corroborate with those from other authors who analyzed some of these effects using different numerical models (1D and 3D), including the theory of magnetization commutation to estimate the switching time for the sharpened rise time of the output pulse.

In addition, we validated the model proposed by comparing the result with one elsewhere described in the literature,[12] using the 1D form of the LLG equation. The results showed that our model reproduces the response for the output pulse with reasonable accuracy, although all data information is not available in the original publication.

Despite some works in the literature that deal with the 1D form of the LLG equation, this work analyzes the effect of sharpening based on a model using a general formulation developed in Mathematica software, where the parameters can be changed easily and quickly, since the elements were indexed individually, providing a valuable tool to study the phenomena of wave propagation in gyromagnetic lines. It is worth mentioning that the formulation presented here also applies to other geometries, such as stripline and planar waveguides,[25] by using appropriate expressions for the linear capacitance and inductance per unit length as given in Eq. (5) for the coaxial structure.

Furthermore, a model using the 3D form of the LLG equation with axial polarization is under construction to further reduce the output pulse and generate radio frequency, soon new simulations will be carried out, and the results will be used to compare with other numerical and experimental works found in the literature.

SUPPLEMENTARY MATERIAL

See the supplementary material with codes implemented in Mathematica (v. 12.0).

ACKNOWLEDGMENTS

The authors would like to thank the National Institute for Space Research—INPE and the Associated Plasma Laboratory—LABAP for providing the facilities for this research. This work was supported, in part, by CAPES (Grant Nos. 88887.492309/2020-00 and 88887.360820/2019-00), CNPq (Grant No. 306540/2019-3), FAPESP (Grant No. 2018/26086-2), and SOARD/AFSOR–USAF (Grants No. FA9550-18-1-0111 and FA9550-19-1-0225).

AUTHOR DECLARATIONS

Conflict of Interest

The authors have no conflicts to disclose.

DATA AVAILABILITY

The data that support the findings of this study are available from the first author upon reasonable request.

REFERENCES

[1] R. Landauer, "Shock waves in nonlinear transmission lines and their effect on parametric amplification," IBM J. Res. Dev. **4**, 391–401 (1960).
[2] I. G. Katayev, *Electromagnetic Shock Waves* (Lliffe Books Ltd., London, 1966).
[3] R. H. Freeman and A. E. Karbowiak, "An investigation of nonlinear transmission lines and shock waves," J. Phys. D: Appl. Phys. **10**, 633 (1977).
[4] N. Seddon and E. Thornton, "A high-voltage, short-risetime pulse generator based on a ferrite pulse sharpener," Rev. Sci. Instrum. **59**, 2497–2498 (1988).
[5] R. Pouladian-Kari, A. J. Shapland, and T. M. Benson, "Development of ferrite line pulse sharpeners for repetitive high-power applications," in IEE Proceedings H (Microwaves, Antennas and Propagation) (IET Digital Library, 1991), pp. 504–512.
[6] T. M. Benson, R. Pouladian-Kari, and A. J. Shapland, "Novel operation of ferrite loaded coaxial lines for pulse sharpening applications," Electron. Lett. **27**, 861–863 (1991).
[7] R. J. Baker, D. J. Hodder, B. P. Johnson *et al.*, "Generation of kilovolt-subnanosecond pulses using a nonlinear transmission line," Meas. Sci. Technol. **4**, 893 (1993).
[8] G. Branch and P. W. Smith, "Fast-rise-time electromagnetic shock waves in nonlinear ceramic dielectrics," J. Phys. D: Appl. Phys. **29**, 2170 (1996).
[9] J. E. Dolan, H. R. Bolton, and A. J. Shapland, "Development of 60 ps rise-time ferrite-loaded coaxial line," Electron. Lett. **33**, 2049–2050 (1997).
[10] J. O. Rossi, F. S. Yamasaki, J. J. Barroso *et al.*, "RF generation using a compact bench gyromagnetic line," Rev. Sci. Instrum. **93**, 024704 (2022).
[11] A. F. G. Greco, J. O. Rossi, J. J. Barroso *et al.*, "Numerical simulation of a gyromagnetic NLTL using an LC discrete line model," in *IEEE International Conference on Plasma Science (ICOPS)* (IEEE, 2021), pp. 1.
[12] J. E. Dolan, "Simulation of ferrite-loaded coaxial lines," Electron. Lett. **29**, 762–763 (1993).
[13] Wolfram Research, Inc., Mathematica, Version 12.1, Champaign, IL, 2020.
[14] J. E. Dolan, "Simulation of shock waves in ferrite-loaded coaxial transmission lines with axial bias," J. Phys. D: Appl. Phys. **32**, 1826 (1999).
[15] W. Tie, C. Meng, C. Zhao, X. Lu *et al.*, "Optimized analysis of sharpening characteristics of a compact RF pulse source based on a gyro-magnetic nonlinear transmission line for ultrawideband electromagnetic pulse application," Plasma Sci. Technol. **21**, 095503 (2019).
[16] J. E. Dolan, "Effect of transient demagnetisation fields on coherent magnetic switching in ferrites," IEE Proc.-A: Sci., Meas. Technol. **140**, 294–298 (1993).
[17] A. Vasellar, "Experimentation and modeling of pulse sharpening and gyromagnetic precession within a nonlinear transmission line," M.S. thesis, Texas Tech University, Lubbock, TX, 2011.
[18] E. M. Gyorgy, "Rotational model of flux reversal in square loop ferrites," J. Appl. Phys. **28**, 1011–1015 (1957).

[19]R. M. Perks and J. E. Dolan, "Modelling electromagnetic shock lines using finite difference time-domain (FDTD) and transmission line matrix (TLM)-type models," in *IEE Symposium on Pulsed Power'99 (Digest No. 1999/030)* (IET, 1999), pp. 27/1–27/4.
[20]M. Weiner and L. Silber, "Pulse sharpening effects in ferrites," IEEE Trans. Magn. **17**, 1472–1477 (1981).
[21]S. Furuya, H. Matsumoto, H. Fukuda *et al.*, "Simulation of nonlinear coaxial line using ferrite beads," Jpn. J. Appl. Phys. **41**, 6536 (2002).
[22]L. Huang, J. Meng, D. Zhu, and Y. Yuan, "Field-line coupling method for the simulation of gyromagnetic nonlinear transmission line based on the Maxwell-LLG system," IEEE Trans. Plasma Sci. **48**, 3847–3853 (2020).
[23]J. E. Dolan and H. R. Bolton, "Shock front development in ferrite-loaded coaxial lines with axial bias," IEE Proc.-A: Sci., Meas. Technol. **147**, 237–242 (2000).
[24]Y. Cui, J. Meng, L. Huang *et al.*, "Operation analysis of the wideband high-power microwave sources based on the gyromagnetic nonlinear transmission lines," Rev. Sci. Instrum. **92**, 034702 (2021).
[25]D. V. Reale, J. M. Parson, A. A. Neuber, J. C. Dickens, and J. J. Mankowski, "Investigation of a stripline transmission line structure for gyromagnetic nonlinear transmission line high power microwave sources," Rev. Sci. Instrum. **87**(3), 034706 (2016).